Spatial decorrelation of wind noise by porous microphone windscreens

Sipei Zhao and Eva Cheng
School and Engineering, RMIT University, Melbourne, Australia
Xiaojun Qiu and Ian Burnett
Centre for Audio, Acoustics and Vibration, Faculty of Engineering and IT, University of Technology Sydney, Sydney, Australia
Jacob Chia-chun Liu
Department of Water Resources and Environmental Engineering, Tamkang University, Taiwan

This paper explores the wind noise reduction mechanism of porous microphone windscreens by investigating the spatial correlation of wind noise. The spatial structure of the wind noise signal is studied by calculating the magnitude squared coherence of the pressure measured with two microphones at various separation distances. It is found that the coherence of the two signals decreases with the separation distance and the wind noise is spatially correlated only within a certain distance less than the turbulence wavelength. Comparing the spatial coherence between the wind noise outside and inside a porous microphone windscreen with that without the windscreen shows that the coherence is reduced significantly in a certain frequency range where the windscreen diameter is approximately 2 to 4 times of the turbulence wavelengths, which corresponds to the most effective wind noise reduction frequency range of the windscreen. Experiment results with a fan are presented to support the simulations. It is concluded that the wind noise reduction mechanism of porous microphone windscreens is related to the spatial decorrelation effect on the wind noise signals provided by the porous material and structure.

1. Introduction

Wind noise due to the pressure fluctuations on microphones is inevitable for acoustic measurements with flow presence, such as in outdoor atmosphere and in the ventilation system in ducts (Mcguinn et al., 1997; Raspet and Webster, 2015). Previous research shows that the fluctuation wake due to the interaction between microphone and flow is the dominant wind noise source for indoor low-turbulence conditions, whereas the dominant source of pressure fluctuations at the microphone in outdoor atmosphere is the intrinsic turbulence in the incoming flow (Morgan and Raspet, 1992; Strasberg, 1988). Various methods have been explored in the past to attenuate the wind noise, among which porous microphone windscreens are widely used (Raspet et al., 2006). This paper is devoted to understanding the wind noise reduction mechanism of porous microphone windscreens.

Porous microphone windscreens with different diameter have been extensively studied experimentally in both indoor and outdoor environments. Wang et al. (2012) measured the self-noise of microphone windscreens in an anechoic wind tunnel and found that the wind noise is generally more effectively attenuated by windscreens with larger diameters, but windscreens with diameter 60 mm and 90 mm showed similar performance. Lin et al. (2014) measured the wind noise reduction of different types of windscreens in the low frequency range from 20 Hz to 200 Hz, finding that the noise reduction of a single layer fabric windscreen (40 cm diameter) is much better than the spherical windscreens (7 cm and 20 cm diameter) and double layer (30 cm and 40 cm diameter) windscreens for wind speeds above 2.0 m/s.

In addition to these experimental studies, different theoretical models have been proposed to investigate the performance of microphone windscreens. Phelps (1938) calculated the pressure inside microphone windscreens by averaging the pressure fluctuations on the windscreen surface based on the assumption that the air flow is irrotational and the windscreen is a rigid sphere. Similarly, with the smooth rigid sphere model, Zheng and Tan (2003) investigated the Reynolds number effects on the wind noise reduction performance of spherical microphone windscreens. However, the real microphone windscreens are mostly made of porous materials and far from the smooth rigid sphere. To narrow the gap between the smooth rigid sphere model and the real windscreens, Xu et al. (2011) modelled the windscreen as porous materials in numerical simulations and investigated the effect of the windscreen shape on the wind noise reduction performance. They found that the horizontal ellipse windscreen with medium flow resistivity provided the most effect wind noise reduction.

Using a different approach, Van Den Berg (2006) analysed the measured wind noise inside microphone windscreens and showed that the windscreen could be considered as a first order low pass filter for pressure variations due to atmospheric turbulence. Raspet et al. (2014) proposed to calculate the pressure inside porous windscreens with the pressure averaged over the windscreen surface which is weighted with the correlation length. The longitudinal and transversal correlation lengths were measured with a pressure tube array inside a 180 mm porous microphone windscreen, and results

show that the predicted pressure level at the centre of the windscreen is lower than the measured wind noise level (Raspet et al., 2014).

Similar to porous microphone windscreens, spatial filters and wind fences with different porosity were used to attenuate the infrasonic wind noise outdoors (Abbott et al., 2015; Hedlin and Raspet, 2003). Abbot and Raspet (2015) developed a calculation model to predict the wind noise below 50 Hz in a 2.9 m high and 5.0 m diameter wind fence, and showed that the low frequency wind noise is only due to turbulence-shear interaction in the undisturbed region while the higher frequency wind noise is due to a combination of the turbulence-turbulence and turbulence-shear interactions inside the enclosure and the turbulence interactions on the surface of the enclosure.

Most of the above studies focused on the wind noise inside the windscreen measured with a single microphone, without considering the spatial structure of the wind noise. Recent wind noise measurements with microphone arrays showed that the wind noise remains somewhat stable over a finite distance and time (Bass et al., 1995). Shields (2005) employed a three-axis orthogonal microphone array with ten sensors in each arm to measure the outdoor wind noise and studied the time domain correlation as a function of sensor separation in the frequency range from 0.05 Hz to 50 Hz. The results show that the correlation varies as $e^{-3.2X}\cos(2\pi X)$ in the downwind direction and decays as e^{-7Y} in the crosswind direction, where X and Y are the separation in wavelengths in the downwind and crosswind direction, respectively.

Wilson et al. (2007) measured the outdoor wind noise with a 7×7 planar horizontal microphone array and found that the wind noise is substantially correlated for the microphone separations smaller than the size of the turbulent eddies while the wind noise becomes nearly uncorrelated when the microphone separation increases beyond the eddy size. In a further study, Wilson and White (2010) compared the spatial and temporal structure of wind noise and acoustic signal measured with the planar microphone array using the wavelet cross spectrum method and formulated a Gaussian-mixture-model classifier to distinguish between blasting sounds, music and wind noise.

This paper investigates the wind noise reduction mechanism of porous microphone windscreens by examining the effect of the porous windscreens on the spatial structure of wind noise (signal). The spatial structure of the wind noise is studied by using the magnitude square coherence of the pressure measured with two microphones at various separation distances first, and then the wind noise reduction with porous microphone windscreens is investigated. Finally, the spatial coherence between the wind noise outside and inside the porous windscreens are calculated to investigate the wind noise reduction mechanism. Both numerical and experimental results show that the porous microphone windscreens are more effective in reducing wind noise in a certain frequency range where the spatial structure of wind noise is decorrelated by the porous windscreen.

2. Simulation model

The diagram of the simulation model is shown in Fig. 1, where a uniform air flow with mean speed U enters the computation domain from the right boundary. The computation domain is 34D in the downwind direction and 10D in the crosswind direction. Five solid cylinders are placed upstream to generate turbulence. The diameter and the interval between cylinders are both D and the solid cylinder array is 4D from the flow inlet boundary. Two sets of simulations are performed.

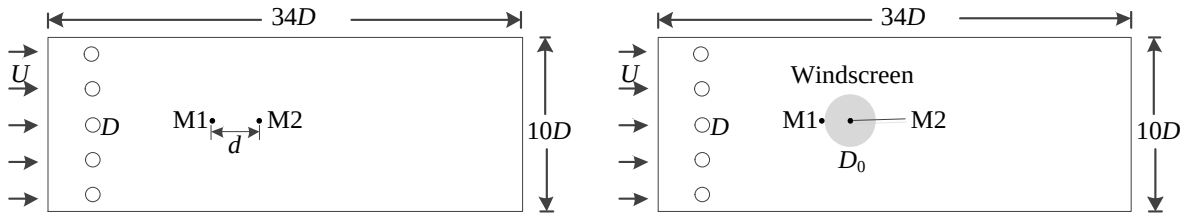

(a) (b)

Fig. 1. Diagram of the simulation model (a) without and (b) with microphone windscreen.

In the first set of simulations in Fig. 1(a), there is no microphone windscreen and the pressure fluctuations at two microphone locations M1 and M2 with various separation distances are monitored to study the spatial structure of wind noise. The fluid flow is described by the Navier-Stokes equations for viscous incompressible flow (Currie, 2013),

$$\nabla \cdot \mathbf{u} = 0 \tag{1}$$

$$\frac{\partial \mathbf{u}}{\partial t} + (\mathbf{u} \cdot \nabla)\mathbf{u} = -\frac{1}{\rho}\nabla p + \nu \nabla^2 \mathbf{u} \tag{2}$$

where $\mathbf{u}$ is the velocity, p is the pressure, ρ is the fluid density and ν is the viscosity of the fluid.

In the second set of simulations in Fig. 1(b), a microphone windscreen of diameter D_0 (grey circle in the figure) is placed 10D from the upstream solid cylinder array. The pressure fluctuations outside (at position M1) and inside (at position M2) the microphone windscreen are recorded and compared with that without windscreen to investigate the effect of the microphone windscreen on the spatial structure of the wind noise. The microphone windscreen is modelled as porous medium, inside which the fluid flow is governed by the continuity equation and the momentum conservation equation proposed by Nithiarasu et al. (Nithiarasu et al., 1997),

$$\nabla \cdot \mathbf{u} = 0 \tag{3}$$

$$\frac{1}{\phi}\frac{\partial \mathbf{u}}{\partial t} + \frac{1}{\phi^2}(\mathbf{u} \cdot \nabla)\mathbf{u} = -\frac{1}{\rho}\nabla p + \frac{\nu}{\phi}\nabla^2 \mathbf{u} - \frac{\nu}{K}\mathbf{u} - C|\mathbf{u}|\mathbf{u} \tag{4}$$

where ϕ is the porosity of the porous medium, K is the permeability of the porous medium, and C is the inertial coefficient.

Equations (1) to (4) were solved in FLUENT 16.0 with the boundary conditions of velocity and stress continuity at the windscreen surface. The models were built, and meshed in ANSYS Workbench 16.0, and simulated in ANSYS FLUENT 16.0. In the simulations, the boundary condition of the flow inlet was set to "velocity inlet", the output boundary condition was set to "pressure outlet", the upper and lower boundaries were set as "wall", and the microphone windscreen is modelled as "porous media zone". In the simulations, the diameter of the upstream cylinders was D = 50 mm. The permeability and inertial coefficients were set as $K = 10^{-7}$ m^2 and C = 50 m^{-1}, respectively. For each simulation, the time history of velocity and pressure fluctuations at the monitoring location was recorded for 5 s with a sampling rate of 10 kHz.

To investigate the spatial structure of the wind noise, the Magnitude Squared Coherence (MSC) between the pressure fluctuations recorded at M1 and M2 were calculated (Carter et al., 1973),

$$MSC(f) = \frac{|\varphi_{12}(f)|^2}{\varphi_{11}(f)\varphi_{22}(f)} \tag{5}$$

where $\varphi_{12}(f)$ is the cross spectral density, $\varphi_{11}(f)$ and $\varphi_{22}(f)$ are the auto spectral density at frequency f. To quantitatively examine the wind noise reduction performance of the windscreens, the Wind Noise Reduction (WNR) are defined as (Abbott et al., 2015)

$$WNR(f) = 10\log_{10}\frac{P_0(f)}{P_{ws}(f)} \quad \text{(dB)} \tag{6}$$

where $P_{ws}(f)$ and $P_0(f)$ are the pressure Power Spectral Density (PSD) with and without windscreen at frequency f, respectively.

3. Simulations

3.1 Spatial structure of the wind noise

In the first set of simulations in Fig. 1(a) where no microphone windscreen is present, the microphone location M1 is fixed and M2 is moved to change the separation distance d from 30 mm to 90 mm with a step of 15 mm. The obtained pressure PSD at location M1 are shown in Fig. 2(a) at various wind speeds from 2 m/s to 14 m/s, and the wind noise is almost flat in the low frequency range while decays rapidly in higher frequency range above 200 Hz. The wind noise increases with the mean wind speed but the rate of noise level change decreases with growing velocity. These two observations are consistent with the wind noise spectra measured in a small anechoic wind tunnel by Alamshah et al. (2015).

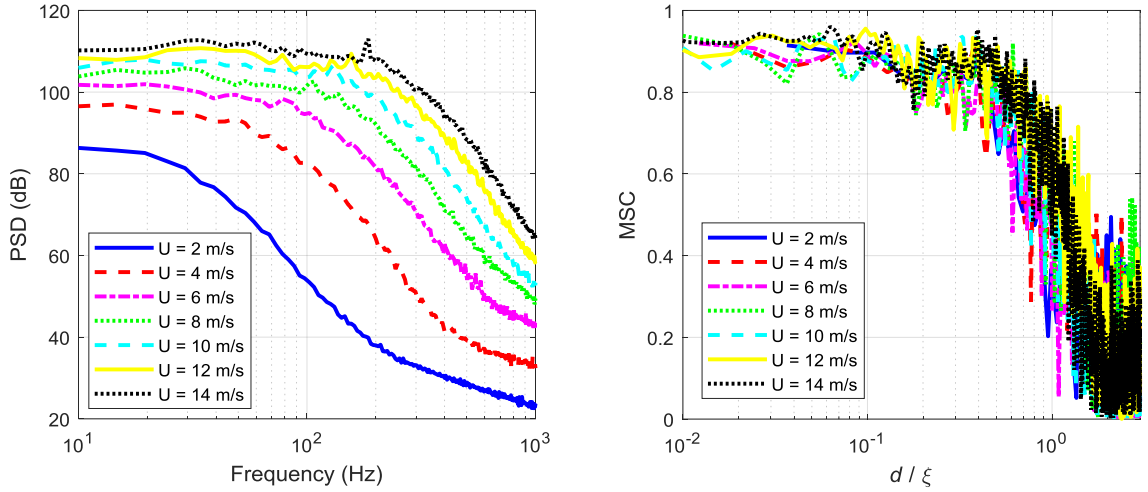

Fig. 2. (a) The Pressure Spectral Density (PSD) as a function of frequency and (b) the Magnitude Squared Coherence (MSC) as a function of the ratio of the separation distance (fixed to 30 mm) to turbulence wavelength (the turbulence wavelength ξ is the variable for the horizontal axis) for the wind noise at different wind speeds

To examine the spatial structure of the wind noise, the MSC between the pressure fluctuations at M1 and M2 are calculated and illustrated in Fig. 2(b) as a function of the separation distance to the turbulence wavelength ratio (d/ξ), where the separation distance d is fixed at 30 mm. The turbulence wavelength is a parameter that is used to characterise the length scale of the turbulent eddies, which can be calculated by $\xi = U/f$ where U is the mean wind speed and f is frequency. A larger turbulence wavelength corresponds to turbulent eddies with larger size. It is also proportional to the inverse of frequency, and large turbulence wavelength corresponds to low frequency

Figure 2(b) shows that when the separation distance is smaller than the turbulence wavelength (i.e. $d/\xi < 1$), the wind noise at location M1 and M2 are coherent, whereas when the separation distance is larger than the turbulence wavelength (i.e. $d/\xi > 1$), the wind noise becomes incoherent. This is reasonable because when the turbulent eddy size is smaller than the separation distance, the instantaneous pressure recorded at location M1 and M2 come from different eddies, hence the pressure signals are incoherent. In contrast, when the turbulent eddy size is larger than the separation distance, the instantaneous pressure at location M1 and M2 are caused by the same eddy, therefore the pressure signals are coherent. It can also be observed from Fig. 2(b) that the MSC at different wind speeds are similar when the turbulence wavelength is larger than the separation distance (i.e. $d/\xi < 1$).

The MSC as a function of the separation distance to wavelength ratio for various separation distances are compared in Fig. 3 for wind speeds U = 4 m/s and U = 10 m/s, where the variable along the horizontal axis is the turbulence wavelength ξ. Figure 3 shows that the pressure at M1 and M2 are incoherent when the separation distance is larger than the turbulence wavelength (i.e. $d/\lambda > 1$)

regardless of the separation distance between microphones. When the turbulence wavelength is larger than the separation distance, the pressure at M1 and M2 are coherent, however the coherence decreases with increasing separation distance, which indicates that large eddies decay with spatial distance as they are advected downstream by the mean flow.

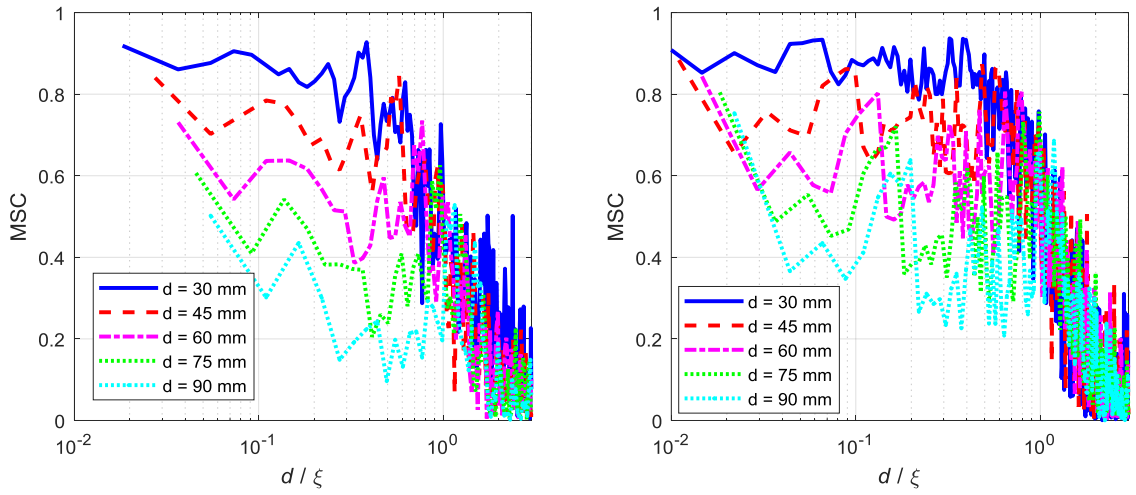

Fig. 3. The Magnitude Squared Coherence (MSC) as a function of the ratio of the separation distance to turbulence wavelength (the turbulence wavelength ξ is the variable for the horizontal axis) for various separation distance for the wind noise at wind speed (a) U = 4 m/s and (b) U = 10 m/s.

3.2 Wind noise reduction by porous microphone windscreens

To investigate the wind noise reduction performance of the porous microphone windscreens with different diameters at various wind speeds, the pressure inside the porous windscreens (M2 in Fig. 1(b)) is simulated and compared with that when the windscreen is absent. The WNR as a function of frequency for a 90 mm porous windscreen is illustrated in Fig. 4(a) for various wind speeds, which shows that the porous windscreen attenuate the wind noise more effectively in a certain frequency range and the centre frequency of this range increases with wind speed. The WNR of porous windscreens with different diameters are compared in Fig. 4(b) at the wind speed U = 4 m/s. Similarly, the wind noise is the more effectively reduced in a certain frequency range which moves to lower frequency region with increasing windscreen diameter.

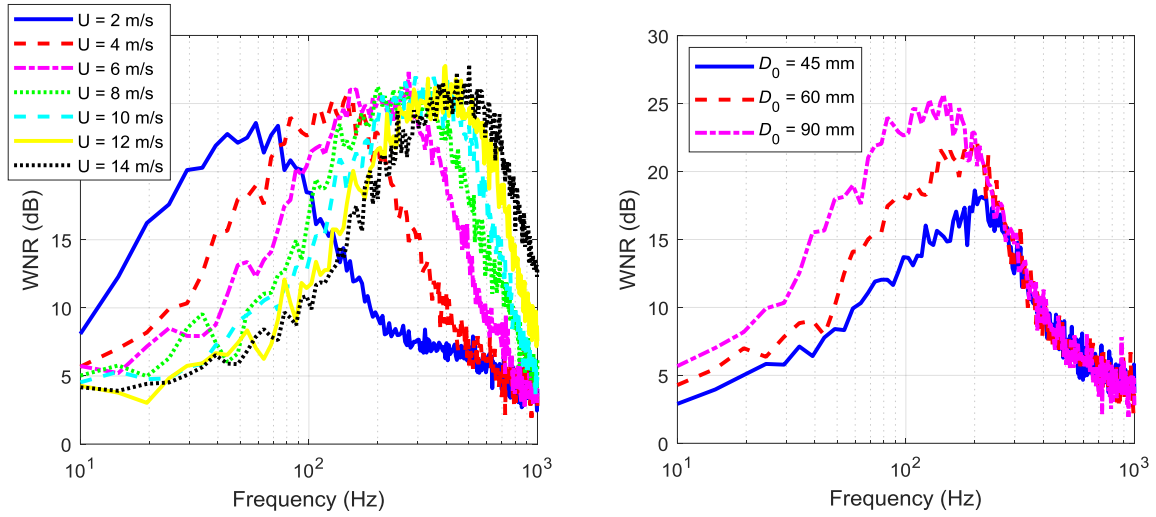

(a) (b)

Fig. 4. The Wind Noise Reduction (WNR) as a function of frequency for (a) 90 mm windscreen at various wind speeds and (b) windscreens with different diameters for the wind noise at wind speed U = 4 m/s.

Figure 5 shows the WNR as a function of the windscreen diameter to turbulence wavelength ratio (D_0/ξ), where the WNR tends to form a single curve and the porous windscreen is most effective in wind noise reduction when the windscreen diameter is approximately 2 to 4 times of the turbulence wavelengths ($2 < D_0/\xi < 4$) regardless of the wind speed and windscreen diameter. When the turbulence wavelength is much larger than the windscreen diameter ($D_0/\xi < 0.1$), the porous windscreen has almost no effect in wind noise reduction. With the turbulence wavelength increasing, the wind noise reduction first increases and then decreases after reaching the maximum. When the turbulence wavelength is much smaller than the windscreen diameter ($D_0/\xi > 10$), the wind noise reduction approaches zero again.

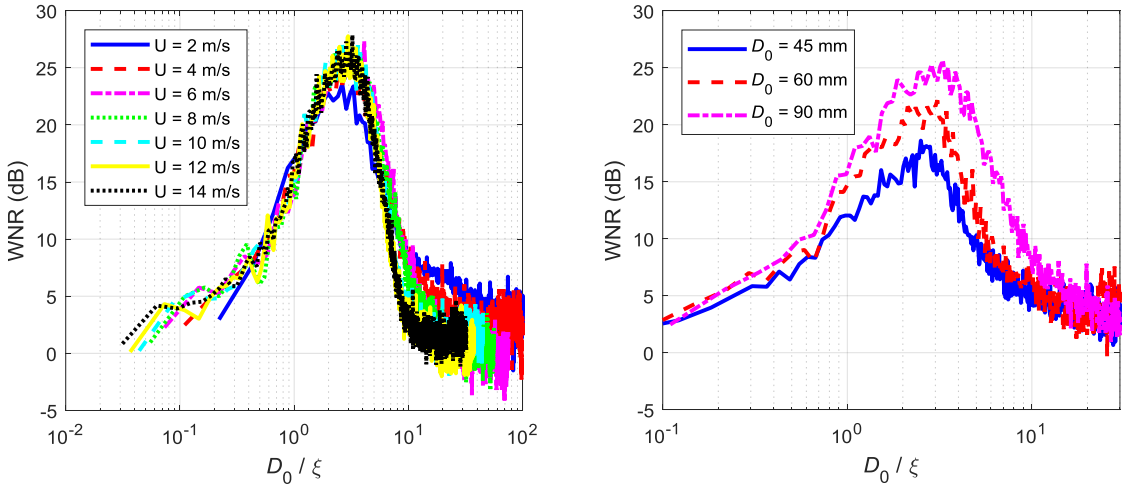

(a) (b)

Fig. 5. The Wind Noise Reduction (WNR) as a function of ration of the windscreen diameter to turbulence wavelength (the turbulence wavelength ξ is the variable for the horizontal axis) for (a) a 90 mm windscreen at various wind speeds and (b) windscreens with different diameters for the wind noise at wind speed U = 4 m/s.

To understand the mechanism of the wind noise reduction by the porous microphone windscreen and the existence of this effective frequency range, the MSC of the pressure outside and inside the 90 mm porous microphone windscreen (M1 and M2 in Fig. 1(b)) is calculated and compared with that when the windscreen is absent. The pressure PSD and MSC in Fig. 6 show that the pressure PSD is reduced significantly in the frequency range between 200 Hz to 600 Hz. This can be more clearly observed in Figs. 6(c) and (d), where the WNR and MSC difference as a function of the windscreen diameter to turbulence wavelength ratio (D_0/ξ) are shown respectively. Figure 6(d) shows that compared to the MSC without the porous windscreen, the MSC with the windscreen is reduced significantly when the windscreen diameter is approximately 2 to 4 times of turbulence wavelength ($2 < D_0/\xi < 4$), which corresponds to the most effect wind noise reduction frequency range in Fig. 6(c).

This observation indicates the mechanism of the wind noise reduction by porous microphone windscreens is related to the spatial deccorelation provided by the porous material and structure. When the turbulence wavelength is much larger than the windscreen, the wind noise is coherent no matter whether the windscreen is present or not, there is barely any reduction in wind noise. When the diameter of the windscreen is between 2 to 4 times of the turbulence wavelength ($2 < D_0/\xi < 4$), the spatial structure of wind noise is docorrelated by the windscreen, the windscreen is most effective in wind noise reduction in this frequency range. When the turbulence wavelength is much smaller than the windscreen, the wind noise itself is incoherent and the windscreen is ineffective.

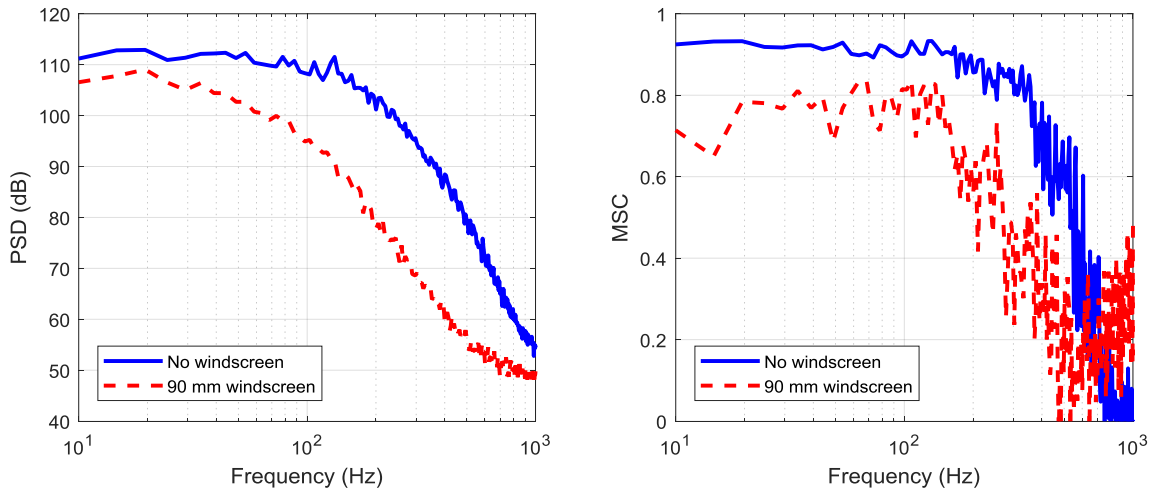

(a) (b)

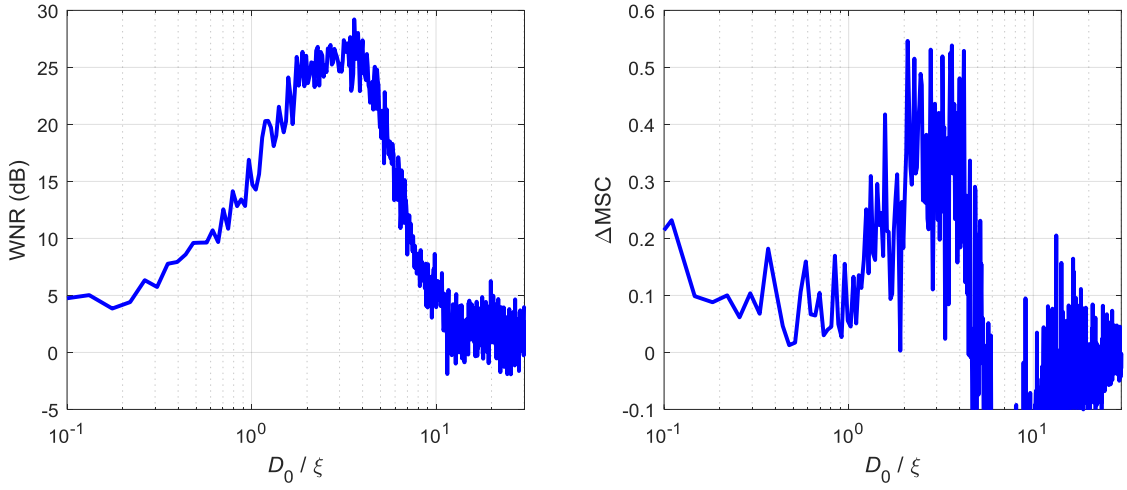

(c) (d)

Fig. 6. (a) The pressure Power Spectral Density (PSD) and (b) the Magnitude Squared Coherence (MSC) as a function of frequency, (c) the Wind Noise Reduction (WNR), and (d) the MSC difference (ΔMSC) as a function of the ratio of the windscreen diameter (90 mm) to the turbulence wavelength (the turbulence wavelength ξ is the variable for the horizontal axis) for the wind noise at wind speed U = 10 m/s.

The simulation results show that the wind noise level increases with the wind speed and the wind noise is spatially coherent at low frequency range where the turbulence wavelength is larger than the separation distance, but the coherence decreases with the separation distance. The porous microphone windscreens are more effective in reducing wind noise in the frequency range where the windscreen diameter is approximately 2 to 4 times of the turbulence wavelength. The wind noise reduction mechanism of the porous microphone windscreen seems related to the decorrelation of the spatial structure of wind noise. The spatial decorrelation is due to the viscous and inertial forces introduced by the porous microphone windscreen, which are shown as the third and fourth terms on the right side of Eq. (4). How is wind noise reduced by the windscreens, how does the spatial decorrelation happen and what is the relationship to the viscous and inertial forces are still not clear, which will be investigated in the future.

4. Experiments

To verify the reliability of the simulations, experiments were performed with a fan in a quiet small meeting room, as shown in Fig. 7(a). The fan and the microphone were approximately 0.8 m above the floor, with a separation distance of 0.5 m. The wind noise was measured with two B&K Type 4189 prepolarized free field 1/2" microphones both equipped with a B&K ZC0032 preamlifier, which were connected to a two channel B&K Type 2270 Hand-held Analyser. The system was calibrated with a B&K Type 4231 calibrator. The wind noise reduction by spherical porous

microphone windscreens with different diameters was measured in the experiments. The arrangements of the microphones without and with a 90 mm porous microphone windscreen are shown in Fig. 7(b) and (c), respectively.

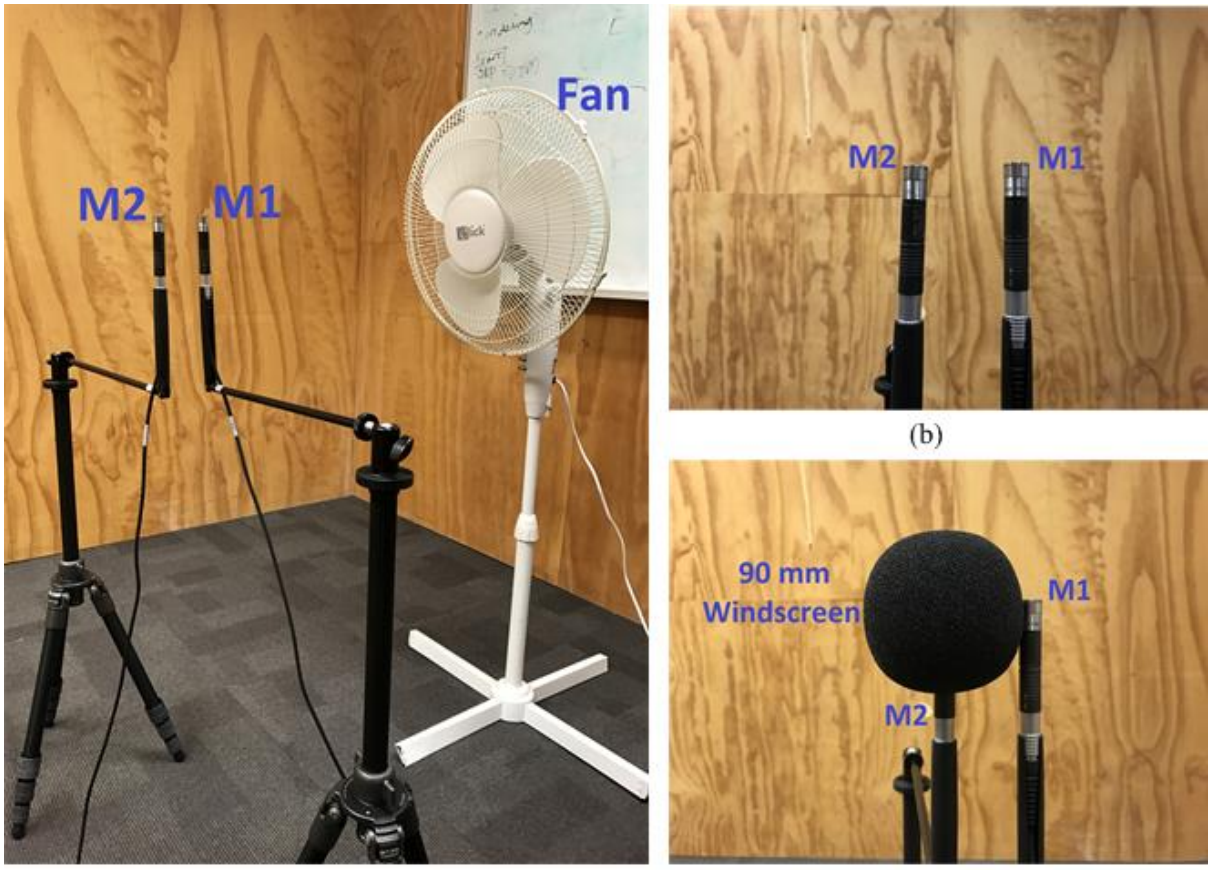

Fig. 7. (a) The experimental setup and the microphone locations (b) without and (c) with a 90 mm windscreen with a porosity of 40 PPI.

In the experiments, the fan ran at its highest speed and the mean wind speed around the microphone was about 3.8 m/s. The wind noise was first measured by a bare microphone at M1 inside the air flow and the background noise was measured by placing the microphone out of the flow but at the same distance from the fan. The wind noise and the background noise spectra of the environment with the fun running are given in Fig. 8(a), which indicates that the wind noise level is much higher than the background noise, hence the measurement results with the microphone placed inside the air flow were primarily due to the wind from the fan. The peak at 62.5 Hz and its harmonics in the background noise are the mechanical noise due to the fan blade.

The spatial structure of the wind noise was first measured without the presence of the microphone porous windscreen as shown in Fig. 7(b). The pressure at two microphones with different separations distance was measured and the MSC are compared in Fig. 8(b). It can be seen that when the

separation distance is larger than the turbulence wavelength (i.e. $d/\xi > 1$), the wind noise at the two microphones are incoherent, while when the separation distance is smaller than the turbulence wavelength, the wind noise is coherent but the coherence decreases with increasing separation distance due to the decay of the turbulent eddies.

It is noteworthy that the wind noise in the simulations is caused by the turbulent wake generated by the upstream solid cylinders, while the wind noise in the experiments is due to the turbulence produced by the fan blade. Therefore the experiment results are not compared with the simulation results quantitatively. However, the trend consistency between the measurement results in Fig. 8 and the simulation results in Fig. 3 can be an evidence of the reliability of the simulations.

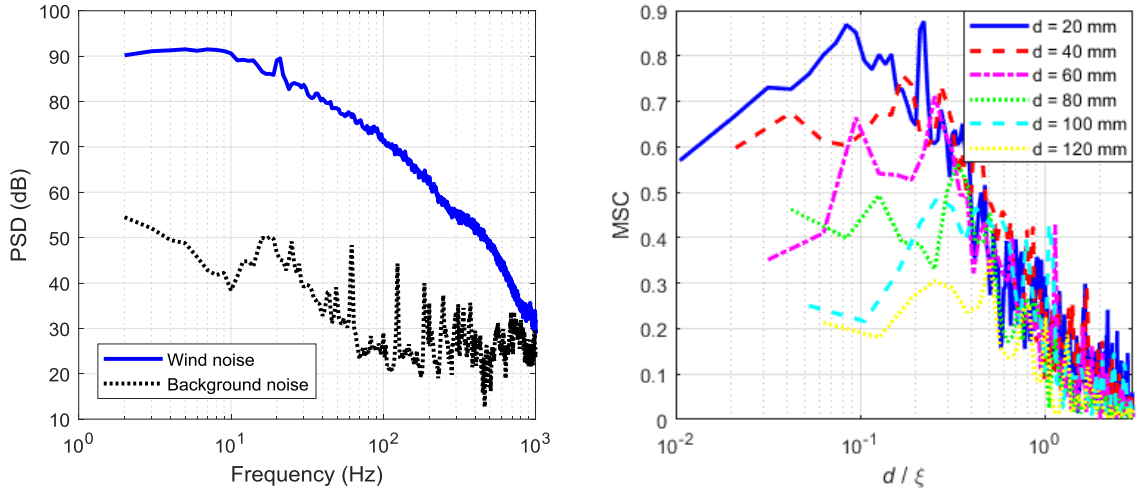

(a) (b)

Fig. 8. (a) The pressure Power Spectral Density (PSD) as a function of frequency and (b) the Magnitude Squared Coherence (MSC) as a function of the separation distance to turbulence wavelength ratio (the turbulence wavelength ξ is the variable for the horizontal axis) measured for the wind noise at the wind speed U = 3.8 m/s in the experiments.

The wind noise reduction by 4 porous microphone windscreens with different diameter was measured and compared in Fig. 9, where the wind speed is U = 3.8. The 45 mm and 90 mm B&K microphone windscreens are UA-1236 and UA-0237, respectively, of which the porosity is unknown. The 60 mm and the other 90 mm windscreens were customized with 40 PPI (Pores Per Inch) polyurethane foam. It is clear from Fig. 9(a) that the porous windscreens are most effective in a certain frequency range and the larger windscreen attenuates more wind noise in lower frequency region. Figure 9(b) presents the WNR as a function of the windscreen diameter to turbulence wavelength ratio (D_0/ξ), which shows that the porous windscreens are most effective in attenuating wind noise when the windscreen diameter is approximately 2 to 4 times of turbulence wavelength ($2 < D_0/\xi < 4$). This is consistent with the simulation results in Fig. 5.

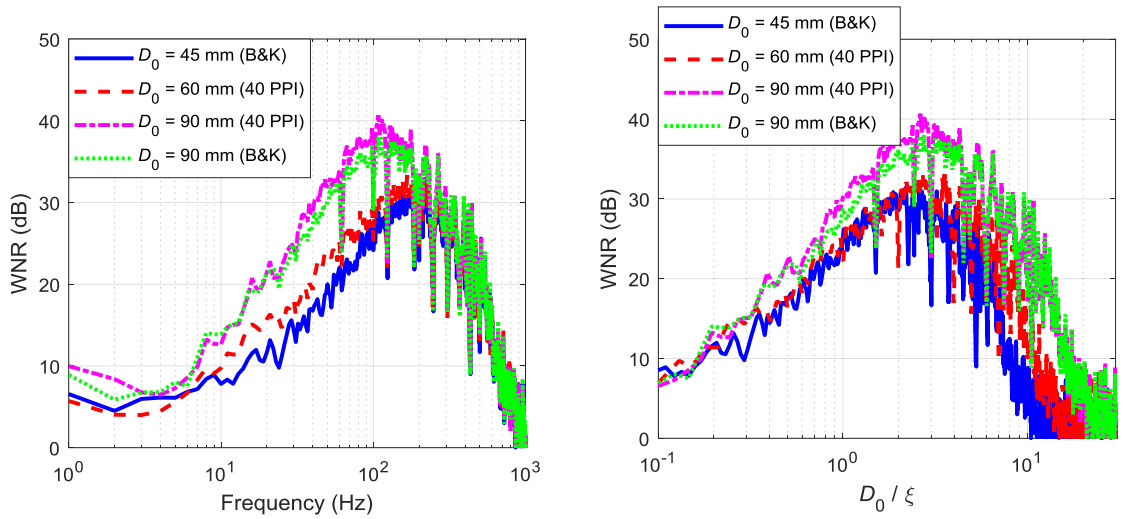

(a) (b)

Fig. 9. The Wind Noise Reduction (WNR) as a function of (a) frequency and (b) the windscreen diameter to turbulence wavelength ratio for windscreens with different diameters measured for the wind noise at the wind speed U = 3.8 m/s.

The pressure PSD inside the 90 mm microphone windscreen (40 PPI) is compared with that without windscreen and the background noise in Fig. 10(a), which shows that the wind noise levels are higher than the background noise; hence the measured noise is primarily due to the wind from the fan. The MSC between the pressures measured at two microphones are shown in Fig. 10(b), which shows that the MSC is reduced the most above 100 Hz. The WNR and the MSC difference as a function of the windscreen diameter to turbulence wavelength ratio (D_0/ξ) are shown in Figs. 10(c) and (d), respectively. It is clear that the MSC with the windscreen is reduced the most when the windscreen diameter is approximately 2 to 4 times of the turbulence wavelengths ($2 < D_0/\xi < 4$), corresponding to the most effect wind noise reduction frequency range in Fig. 10(c). This is also consistent with the simulations in Fig. 6.

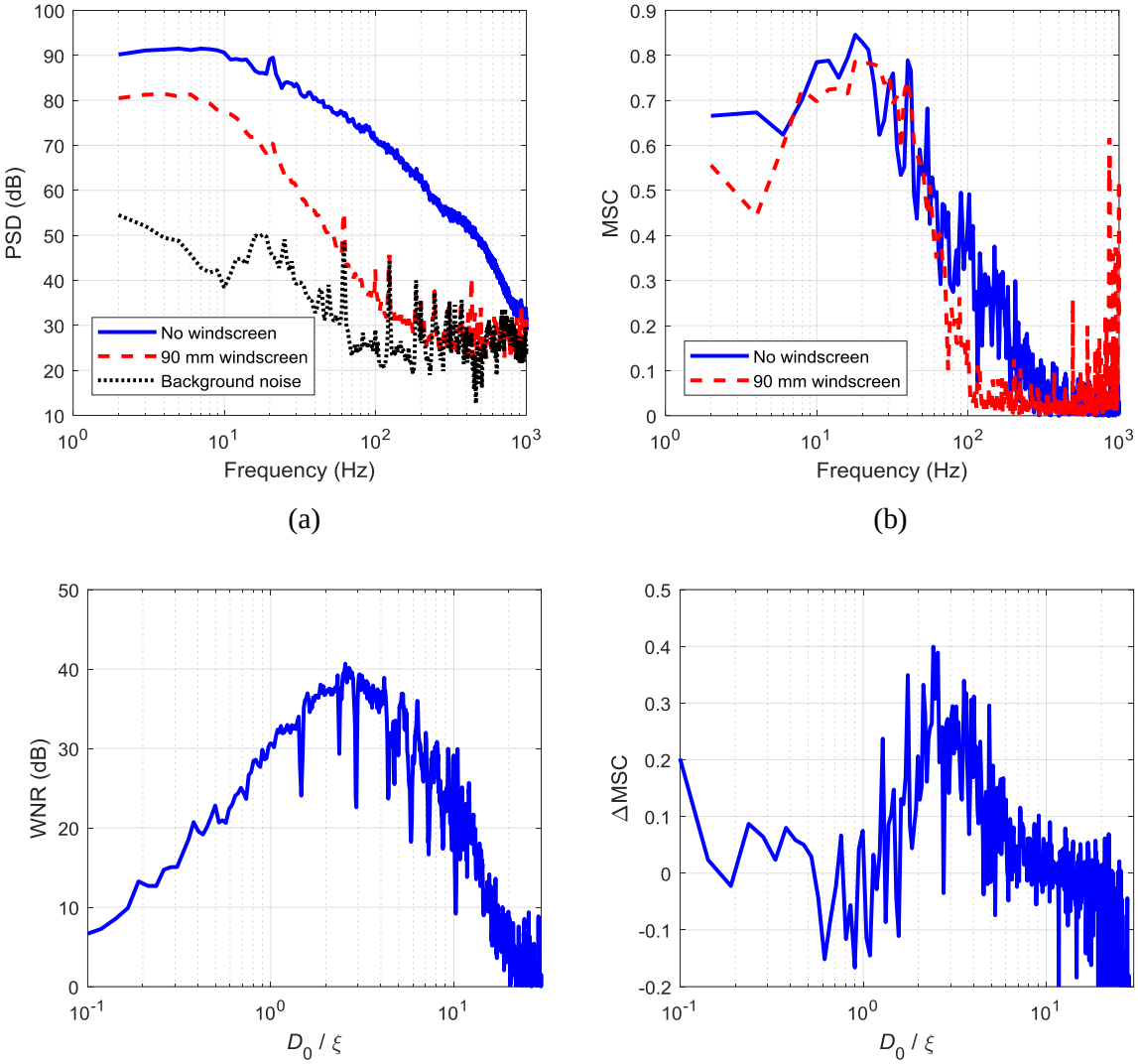

Fig. 10. (a) The pressure Power Spectral Density (PSD), (b) the Wind Nosie Reduction (WNR), (c) the Magnitude Square Coherence (MSC), and (d) the MSC differenrce measured without and with 40 PPI porous microphone windscreens measured for the wind noise at the wind speed U = 3.8 m/s.

5. Conclusions

This paper investigates the spatial structure of wind noise and the physical mechanism of the wind noise reduction by the porous microphone windscreens. Simulation and experiment results show that the wind noise is spatially correlated within a certain distance of the turbulence wavelength. The coherence in the lower frequency range decreases with the separation distance due to the spatial decay of large eddies. The porous microphone windscreens are more effective in reducing the wind noise in a certain frequency range where the windscreen diameter is approximately 2 to 4 times of turbulence wavelength, and the mechanism of the wind noise reduction is related to the decorrelation effect of the spatial structure of wind noise due to the presence of the porous structure of microphone windscreens.

Future work will further investigate the physical mechanism of the wind noise reduction by the porous microphone windscreens and the quantitative relationship between the spatial docorrelation of the wind noise structure and the viscous and inertial forces introduced by porous microphone windscreens.

Acknowledgements

This research was supported under Australian Research Council's Linkage Projects funding scheme (LP140100740).

References

Abbot, J., and Raspet, R. (**2015**). "Calculated wind noise for an infrasonic wind noise enclosure," J. Acoust. Soc. Am., **138**, 332–343. doi:10.1121/1.4922782

Abbott, J., Raspet, R., and Webster, J. (**2015**). "Wind fence enclosures for infrasonic wind noise reduction," J. Acoust. Soc. Am., **137**, 1265–1273. doi:10.1121/1.4908568

Alamshah, V., Zander, A., and Lenchine, V. (**2015**). "Effects of turbulent flow characteristics on wind induced noise generation in shielded microphones," Proc. Acoust. 2015, Hunter Valley, Australia, 1–11.

Bass, H. E., Raspet, R., and Messer, J. O. (**1995**). "Experimental determination of wind speed and direction using a three microphone array," J. Acoust. Soc. Am., **97**, 695–696.

Van Den Berg, G. P. (**2006**). "Wind-induced noise in a screened microphone," J. Acoust. Soc. Am., **119**, 824–833. doi:10.1121/1.2146085

Carter, G. C., Knapp, C. H., and Nuttall, A. H. (**1973**). "Estimation of the magnitude-squared coherence function Via overlapped fast Fourier transform processing," IEEE Trans. Audio Electroacoust., **21**, 337–344. doi:10.1109/TAU.1973.1162496

Currie, I. G. (**2013**). *Fundamental Mechanics of Fluids*, CRC Press, Florida, Fourth Edi., 580 pages.

Hedlin, M. A. H., and Raspet, R. (**2003**). "Infrasonic wind-noise reduction by barriers and spatial filters," J. Acoust. Soc. Am., **114**, 1379–1386. doi:10.1121/1.1598198

Lin, I.-C., Hsieh, Y.-R., Shieh, P.-F., Chuang, H.-C., and Chou, L.-C. (**2014**). "The effect of wind on low frequency noise," Inter.Noise 2014, Melbourne, Australia, 1–12.

Mcguinn, R. S., Lauchle, G. C., and Swanson, D. C. (**1997**). "Low Flow-Noise Microphone for Active Noise Control Applications," AIAA J., **35**, 29–34. doi:10.2514/2.83

Morgan, S., and Raspet, R. (**1992**). "Investigation of the mechanisms of low-frequency wind noise generation outdoors," J. Acoust. Soc. Am., **92**, 1180–1183. doi:10.1121/1.404049

Nithiarasu, P., Seetharamu, K. N., and Sundararajan, T. (**1997**). "Natural convective heat transfer in a fluid saturated variable porosity medium," Inf. J. Heat Man Tramfir, **40**, 395–3967.

Phelps, W. D. (**1938**). "Microphone wind screening," RCA Rev., **111**, 203–212.

Raspet, R., and Webster, J. (**2015**). "Wind noise under a pine tree canopy," J. Acoust. Soc. Am., **137**,

651–659. doi:10.1121/1.4906587

Raspet, R., Webster, J., and Dillion, K. (**2006**). "Framework for wind noise studies," J. Acoust. Soc. Am., **119**, 834–843. doi:10.1121/1.2146113

Raspet, R., Webster, J., and Naderyan, V. (**2014**). "Mechanisms for wind noise reduction by a spherical wind screen," J. Acoust. Soc. Am., **135**, 2381–2381. doi:10.1121/1.4877865

Shields, F. D. (**2005**). "Low-frequency wind noise correlation in microphone arrays," J. Acoust. Soc. Am., **117**, 3489–3496. doi:10.1121/1.1879252

Strasberg, M. (**1988**). "Dimensional analysis of windscreen noise," J. Acoust. Soc. Am., **83**, 544–548. doi:10.1121/1.396148

Wang, L., Zander, A. C., and Lenchine, V. V (**2012**). "Measurement of the self-noise of microphone wind shields," Proc. 18th Aust. Fluid Mech. Conf., Launceston, Australia, 1–10.

Wilson, D., Greenfield, R., and White, M. (**2007**). "Spatial structure of low-frequency wind noise," J. Acoust. …, **122**, EL223-8. doi:10.1121/1.2786608

Wilson, D. K., and White, M. J. (**2010**). "Discrimination of wind noise and sound waves by their contrasting spatial and temporal properties," Acta Acust. united with Acust., **96**, 991–1002. doi:10.3813/AAA.918362

Xu, Y., Zheng, Z., and Wilson, D. (**2011**). "A computational study of the effect of windscreen shape and flow resistivity on turbulent wind noise reduction," J. Acoust. Soc. Am., **129**, 1740–1747. doi:10.1121/1.3552886

Zheng, Z., and Tan, B. (**2003**). "Reynolds number effects on flow/acoustic mechanisms in spherical windscreens," J. Acoust. Soc. Am., **113**, 161–166. doi:10.1121/1.1527927